Chinese Journal of
POLYMER SCIENCE

RESEARCH ARTICLE

https://doi.org/10.1007/s10118-025-3388-5
Chinese J. Polym. Sci. **2025**, *43*, 1483–1495

Tough, Transparent, Self-healing Ionogel with Exceptional Moisture and Impact Resistance

Xiao-Yu Huang[a], Hao-Qi Zhu[a], Luo-Fei Li[a], Tian-Cheng Lv[a], Hao-Yue Li[b], Jun-Jie Gu[b], Wei Wang[a], Bin Xue[a], Hai Lei[c*], and Yi Cao[a,b,d,e*]

[a] *Collaborative Innovation Center of Advanced Microstructures, National Laboratory of Solid State Microstructure, Department of Physics, Nanjing University, Nanjing 210093, China*
[b] *Department of Chemistry and Chemical Engineering, Nanjing University, Nanjing 210023, China*
[c] *School of Physics, Institute for Advanced Study in Physics, Zhejiang University, Hangzhou 310027, China*
[d] *Chemistry and Biomedicine Innovation Center (ChemBIC), Nanjing University, Nanjing 210023, China*
[e] *MOE Key Laboratory of High Performance Polymer Materials & Technology, Nanjing University, Nanjing 210023, China*

Electronic Supplementary Information

Abstract Supramolecular materials that combine toughness, transparency, self-healing, and environmental stability are crucial for advanced applications, such as flexible electronics, wearable devices, and protective coatings. However, integrating these properties into a single system remains challenging because of the inherent trade-offs between the mechanical strength, elasticity, and structural reconfigurability. Herein, we report a supramolecular ionogel designed *via* a simple one-step polymerization strategy that combines hydrogen bonding and ion-dipole interactions in a physically crosslinked network. This dual-interaction architecture enables the ionogel to achieve high tensile strength (9 MPa), remarkable fracture toughness (23.6 MJ·m^{-3}), and rapid self-healing under mild thermal stimulation. The material remains highly transparent and demonstrates excellent resistance to moisture, acid, and salt environments, with minimal swelling and performance degradation. Furthermore, it effectively dissipates over 80 MJ·m^{-3} of energy during high-speed impacts, providing reliable protection to fragile substrates. This study offers a broadly applicable molecular design framework for resilient and adaptive soft materials.

Keywords Ionogel; Physical interaction; Mechanically tough; Self-healing; Impact resistance

Citation: Huang, X. Y.; Zhu, H. Q.; Li, L. F.; Lv, T. C.; Li, H. Y.; Gu, J. J.; Wang, W.; Xue, B.; Lei, H.; Cao, Y. Tough, transparent, self-healing ionogel with exceptional moisture and impact resistance. *Chinese J. Polym. Sci.* **2025**, *43*, 1483–1495.

INTRODUCTION

The development of soft yet tough materials that combine high mechanical robustness, transparency, self-healing capability, and environmental resilience remains a fundamental challenge in polymer science. Such materials are urgently needed in various fields, including personal protection,[1,2] aerospace,[3,4] transportation,[5] military equipment,[6–8] and electronic devices,[9–16] where materials must simultaneously endure mechanical deformation, resist environmental interference, and recover from damage.

Traditional tough polymer networks, including double-network hydrogels,[17–20] nanocomposites[21–27] and hierarchical assemblies,[28–34] often rely on complex structures or chemical crosslinking strategies to dissipate mechanical energy. However, they suffer from critical drawbacks, such as permanent damage under impact, lack of recovery ability, water-induced degradation, and limited design versatility. Supramolecular interactions, such as hydrogen bonds, ion-dipole interactions, and cation-π interactions, have shown promise in enabling dynamic reversibility, energy dissipation, and self-repair. Nevertheless, the incorporation of only a single type of supramolecular interaction in materials may lead to deficiencies in the mechanical strength or ductility, while also restricting the multifunctional applicability of the material.

In recent advances, synergistic design that combines multiple supramolecular interactions has emerged as a powerful strategy to construct soft materials with both toughness and dynamic healing capability.[35–38] This mechanism enables the rapid reformation of the polymer network post-deformation while maintaining strong cohesive forces that enhance mechanical toughness and environmental stability. More importantly, polymers employing synergistic multiple supramolecular interactions not only break the longstanding trade-off between strength and flexibility but also endow the materials with functional application potential.[39–42]

* Corresponding authors, E-mail: leihai@zju.edu.cn (H.L.)
E-mail: caoyi@nju.edu.cn (Y.C.)

Received May 10, 2025; Accepted May 28, 2025; Published online July 18, 2025

Inspired by these advances, we report a tough, transparent, impact-resistant ionogel synthesized through a facile one-step polymerization route. By integrating polymerizable ionic liquids, acrylate, and acrylamide-based precursors, we constructed a physically crosslinked network governed by a combination of hydrogen bonding and ion-dipole interactions. The combination of slightly weaker ion-dipole interactions and slightly stronger hydrogen bonds not only effectively enhanced the mechanical properties of the material but also served as energy-dissipating units during deformation, thereby imparting excellent impact resistance to the material. This dual-interaction design imparts the ionogel with exceptional fracture toughness (about 23.6 MJ·m^{-3}), high tensile strength (about 9 MPa), excellent transparency (>94%), and rapid self-healing under mild thermal stimulation. Spectroscopic analysis and density functional theory (DFT) simulations elucidated the reversible and cooperative nature of the supramolecular interactions, explaining the observed balance between strength, elasticity, and recovery.

Furthermore, owing to its fluorinated ionic structure and cohesive network integrity, the ionogel showed remarkable environmental resilience, with negligible swelling in humid or aquatic conditions, and outstanding impact energy dissipation under high-speed loading. This study provides a generalizable supramolecular strategy for designing multifunctional soft materials that combine toughness, resilience, and recoverability, potentially enabling new generations of durable flexible devices and protective materials.

EXPERIMENTAL

All experimental details are provided in the electronic supplementary information (ESI).

RESULTS AND DISCUSSION

Design and Fabrication of the Ionogel

To achieve a material that is not only tough and transparent but also capable of rapid self-healing and withstanding mechanical impact in humid environments, we designed an ionogel guided by a supramolecular strategy. Specifically, we aimed to combine dynamic hydrogen bonds and stable ion-dipole interactions within a physically crosslinked network, allowing the material to dissipate energy effectively while maintaining structural integrity.

The synthesis process and specific components of the ionogel are shown in Fig. 1. A simple one-step method was adopted for ionogel preparation, in which all monomer components, ionic liquid additives, and a photoinitiator were uniformly mixed and directly cured under UV irradiation to obtain the sample (Fig. 1a). The polymer network of the ionogel consisted of ethyl acrylate, acrylamide, and methacryloxyethyltrimethyl ammonium bis(trifluoromethanesulfonyl)-imide ([MATAC][TFSI]), with a small amount of butyltrimethylammonium bis(trifluoromethanesulfonyl)imide ([N_{4111}][TFSI]) introduced as a plasticizer to enhance the ductility and energy dissipation capability of the ionogel. Ethyl acrylate served as the primary backbone component, contributing to the flexibility and deformability of the material. The amine groups of acrylamide act as hydrogen bond donors, forming hydrogen bond interactions with other molecules in the polymer chains and thereby improving the strength and toughness of the ionogel. [MATAC] in the polymer chains is derived from the polymerization of its corresponding ionic liquid, with bis(trifluoromethanesulfonyl)imide ([TFSI]) as the anion. The positively charged quaternary ammonium side chains can form ion-dipole interactions with carbonyl dipoles,[43] further enhancing the mechanical properties of the ionogel. The ad-

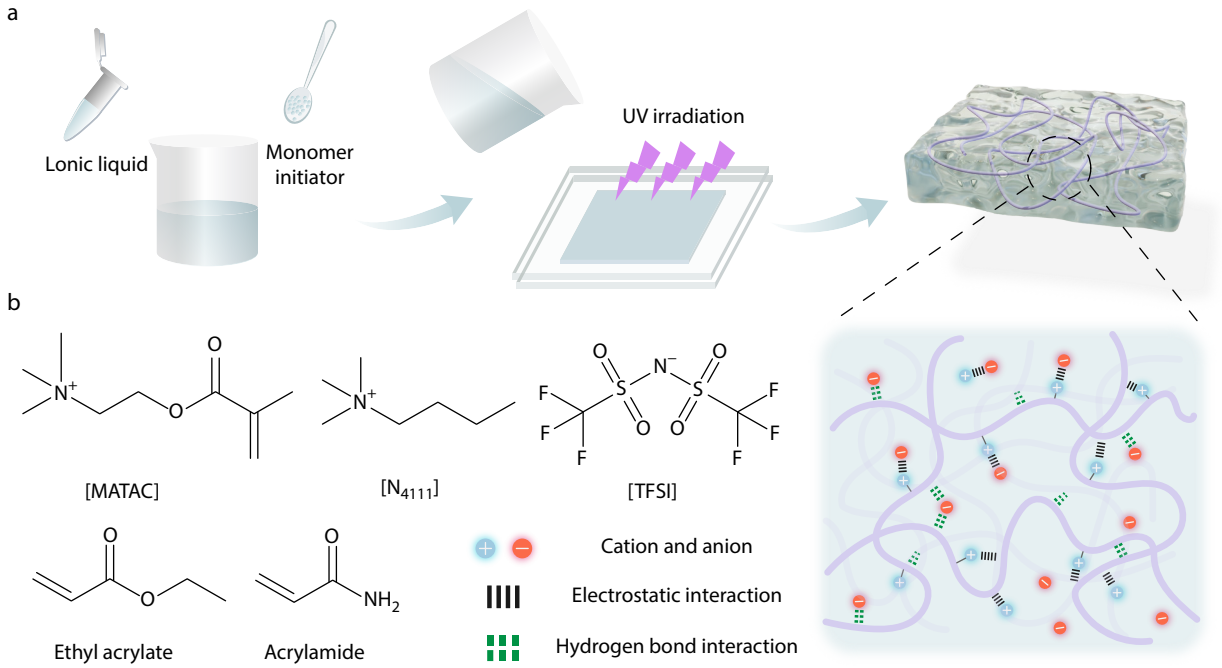

Fig. 1 Preparation process and structural schematic diagram of the ionogel. (a) Preparation process of impact-resistant ionogels; (b) Polymer network structure and specific components of impact-resistant ionogels.

https://doi.org/10.1007/s10118-025-3388-5

ditionally introduced [N_{4111}][TFSI] ionic liquid has a structure similar to that of [MATAC][TFSI] and can also interact well with the polymer network, ensuring that it does not leak under large deformations caused by external forces (Fig. 1b).[44]

Generally, high strength and dynamic recoverability are mutually exclusive in polymer systems.[45–47] High strength typically requires a high crosslinking density, which restricts the polymer chain mobility and consequently hinders chain rearrangement for self-recovery. Moreover, in solvent-free or low-solvent systems, tightly packed polymer chains further limit interfacial chain rearrangement, reducing the self-healing capability. However, in our ionogel system, despite the dense chain packing, the abundant dynamic non-covalent interactions between the polymer chains enable the material to maintain high strength and energy dissipation while exhibiting excellent reversibility and dynamic behavior, ensuring outstanding recovery and self-healing properties.

Molecular Mechanism and Spectroscopic Validation

As illustrated in Fig. 2(a), the impact-resistant ionogel exhibits two key interactions. Ion-dipole interactions between positively charged quaternary ammonium cations and electronegative carbonyl oxygen atoms, and hydrogen bonding between the amine groups (hydrogen bond donors) of the acrylamide and carbonyl groups. These interactions are common among polymers. For example, ion-dipole interactions enhance the stability and dynamics of ether-, carbonyl-, or fluorine-containing polymers, while hydrogen bonding in polyurea or polyacrylic acid significantly strengthens materials.[48–50]

First, we investigated the ion-dipole interactions using ^{1}H-NMR spectroscopy (Fig. 2b). The peak at 3.133 ppm, assigned to the $-N(CH_3)_3^+$ protons of [MATAC], shifted downfield upon mixing with ethyl acrylate or acrylamide, indicating that

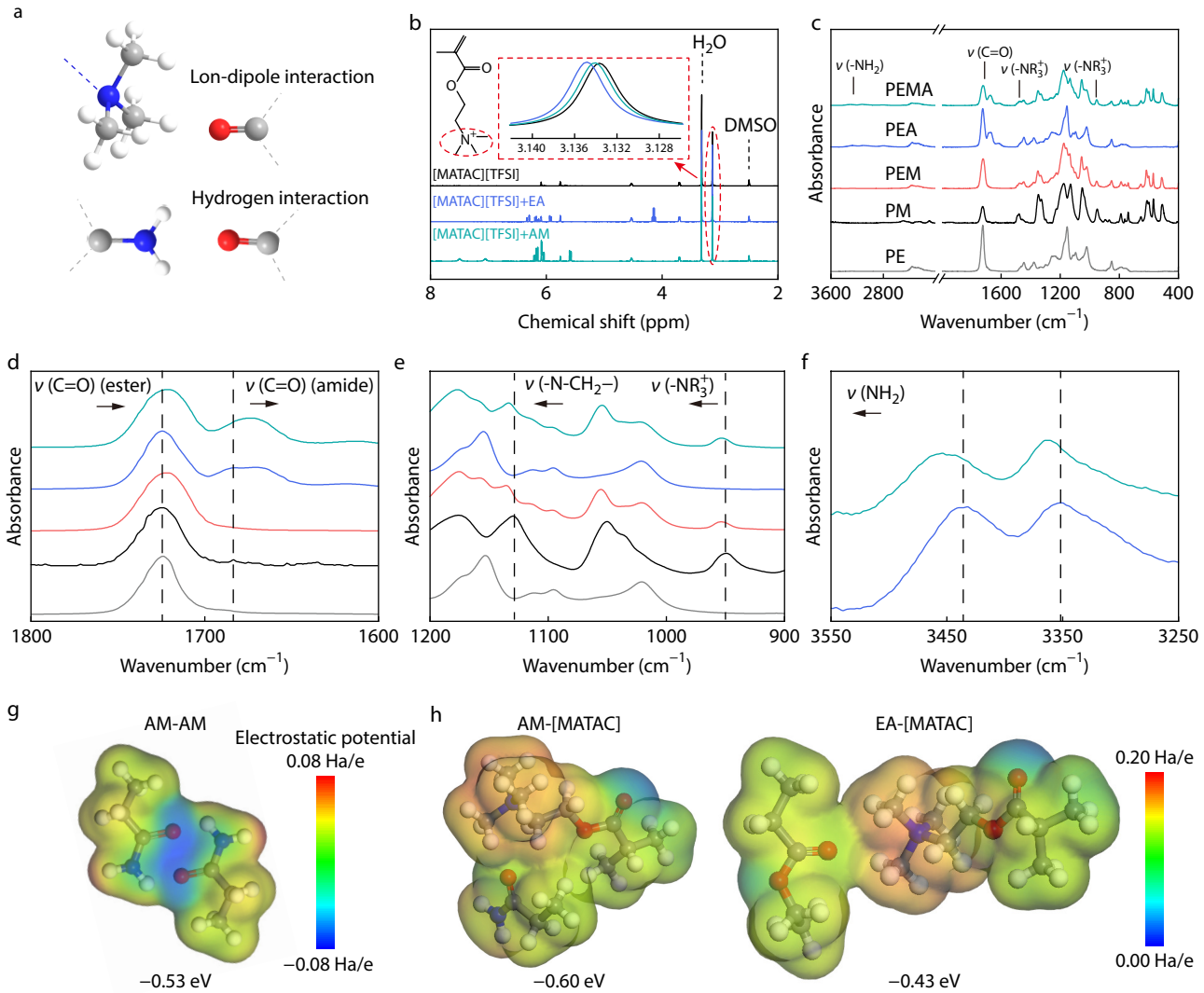

Fig. 2 Spectroscopic analysis and theoretical calculations. The grey, white, red, and blue spheres represent carbon, hydrogen, oxygen, and nitrogen atoms, respectively. (a) Schematic diagram of the hydrogen bond and ion-dipole interactions in the ionogel; (b) The ^{1}H-NMR spectra related to ion-dipole interactions; (c) The full FTIR spectra of different ionogel components (Here, P denotes poly, while E, A and M represent ethyl acrylate, acrylamide and [MATAC][TFSI], respectively); (d) The carbonyl absorption peaks of ethyl acrylate and [MATAC]; (e) The absorption peaks associated with the quaternary ammonium cation; (f) The amide absorption peaks of acrylamide; The structures and corresponding binding energies of the (g) hydrogen bonds and (h) ion-dipole interactions calculated by density functional theory.

https://doi.org/10.1007/s10118-025-3388-5

the protons became more deshielded and supported the formation of ion-dipole interactions.[51] To further verify the interactions in our ionogel, we conducted FTIR analysis of poly(ethyl acrylate) (PE) and poly [MATAC][TFSI] (PM) with varying compositions (Fig. 2c). As shown in Fig. 2(d), the C=O stretching vibration of ethyl acrylate appeared at 1724 cm^{-1}. Due to the different chemical environments of the carbonyl group, the C=O stretching vibration peak of acrylamide appears at 1680 cm^{-1}. Notably, another absorption peak of nearly equal intensity was observed at 1670 cm^{-1}, which is attributed to the carbonyl group of acrylamide forming hydrogen bonds with its amide group. After the addition of [MATAC][TFSI], the carbonyl absorption peak of ethyl acrylate shifted from 1724 cm^{-1} to 1721 cm^{-1}, indicating an interaction between the cation and ethyl acrylate.[52] In addition, no characteristic vibrational peak corresponding to C=C stretching was observed at 1650 cm^{-1}, indicating that the monomers were nearly completely polymerized.

In poly[MATAC][TFSI], the absorption peaks at 948 and 1128 cm^{-1} correspond to the vibrations of the quaternary ammonium cation $-N(CH_3)_3^+$ and $-N-CH_2-$, respectively (Fig. 2e).[53] Upon incorporating [MATAC][TFSI] into PE and PE elastomers containing acrylamide, both the absorption peaks shifted to higher wavenumbers. Additionally, the vibration peak of the amide group in acrylamide undergoes a blue shift (Fig. 2f), confirming the formation of ion-dipole interactions between the positively charged quaternary ammonium cation and the C=O group, as well as the resulting reduction in the hydrogen bond density.

Density functional theory (DFT) calculations were performed to optimize the structures and electrostatic potentials of the interacting species. As shown in Fig. 2(g), hydrogen bonding between the amine (donor) and carbonyl (acceptor) groups lowers the energy of the system. Similarly, the binding energies for [MATAC]-ethyl acrylate and [MATAC]-acrylamide reflected ion-dipole interactions (Fig. 2h). Notably, the binding energy of [MATAC]-acrylamide exceeded that of acrylamide-acrylamide hydrogen bonding, indicating a preference for acrylamide to interact with [MATAC]. Experimentally, we observed that acrylamide dissolved more readily in the [MATAC][TFSI]-containing precursor solutions and resisted precipitation upon cooling. These findings confirm that hydrogen bonding and ion-dipole interactions critically influence the properties of the ionogel. The binding energy of EA-[MATAC] is lower than that of the hydrogen bonds between the AM molecules and the ion–dipole interactions between AM and [MATAC][TFSI]. Therefore, in addition to serving as the main component of the elastic network, EA may also participate in ion-dipole interactions to some extent, thereby enhancing the intrinsic mechanical strength and energy dissipation of the ionogel.

The presence of abundant and dense non-covalent interactions in ionogels can immobilize the polymer chain segments, which is unfavorable for energy dissipation. Additionally, the extensive non-covalent interactions between the polymer chains can mimic the effect of covalent crosslinking, reducing the extensibility of the polymer. Therefore, we introduced a small amount of $[N_{4111}][TFSI]$ ionic liquid into the ionogel to enhance the mobility and dynamics of the chain segments. Notably, the $[N_{4111}][TFSI]$ cation shares partial structural similarity with the [MATAC] cation, as both contain positively charged quaternary ammonium side chains. Based on theoretical calculations, the $[N_{4111}]$ cation also formed ion-dipole interactions with both ethyl acrylate and acrylamide within the ionogel (Fig. S1 in ESI). On the one hand, this helps retain the ionic liquid within the polymer network without leakage. However, because $[N_{4111}][TFSI]$ binding to the polymer chains will not form crosslinks, the ion-dipole interactions involving the $[N_{4111}]$ cation do not contribute to the mechanical strength of the ionogel. Instead, they increase the spacing of the polymer chains, making the network more loosely structured, leading to a reduction in the ionogel strength.

As shown in Fig. S2 (in ESI), we compared the effects of varying the $[N_{4111}][TFSI]$ content on the mechanical properties of the ionogels. It was observed that as the $[N_{4111}][TFSI]$ content increased, the fracture strength of the ionogel significantly decreased from 3.49 MPa to 0.62 MPa. Concurrently, the loosening of the polymer network also resulted in a substantial reduction in Young's modulus, dropping from 20.88 MPa to 2.70 MPa. Considering these effects, we fixed the $[N_{4111}][TFSI]$ content to 10 wt%. Under these conditions, the ionogel exhibited a balanced combination of mechanical strength, toughness, and extensibility.

Mechanical Properties Regulation of Ionogels

Next, we thoroughly investigated the influence of monomer composition on the mechanical properties of the ionogels. To demonstrate the universality of the system, acrylamide (AM) and methacrylamide (MAM) were used as hydrogen bond donors in the materials, respectively. The presence of the *α*-methyl group in methacrylamide further enhances the rigidity of the polymer chains and the stability of hydrogen bonds,[54] its solubility in solvents is generally lower than that of acrylamide. Consequently, owing to solubility limitations, the amount of methacrylamide used in our ionogels was also lower than that of acrylamide. To distinguish them, we designated these ionogels as PEM_xA_yN (containing acrylamide) and PEM_xM_yN (containing methacrylamide), where *x* represents the mass fraction of [MATAC][TFSI] relative to the total monomer mass and *y* denotes the mass fraction of acrylamide or methacrylamide relative to the total monomer mass.

We first examined the effect of varying the [MATAC][TFSI] content (0 wt%–25 wt%) on the mechanical properties of the ionogels. Considering factors such as mechanical strength and material homogeneity, the mass fractions of acrylamide and methacrylamide in the ionogels were set to 10 wt% and 5 wt%, respectively. By adjusting the mass fraction of [MATAC][TFSI], we obtained a series of ionogels with distinct mechanical behaviors. As shown in Fig. 3(a), all the PEMAN ionogels exhibited robust mechanical strength, good extensibility, and strain-hardening behavior resembling chemically crosslinked networks. As expected, increasing the [MATAC][TFSI] content led to a higher density of ion-dipole interactions, resulting in greater tensile strength, higher Young's modulus, and reduced elongation. When the [MATAC][TFSI] content increased from 0 wt% to 25 wt%, the fracture stress of the ionogels rose from 2.46 MPa to 9.00 MPa, while the fracture strain decreased from 960% to 401%. Concurrently, Young's modulus increased monotonically from

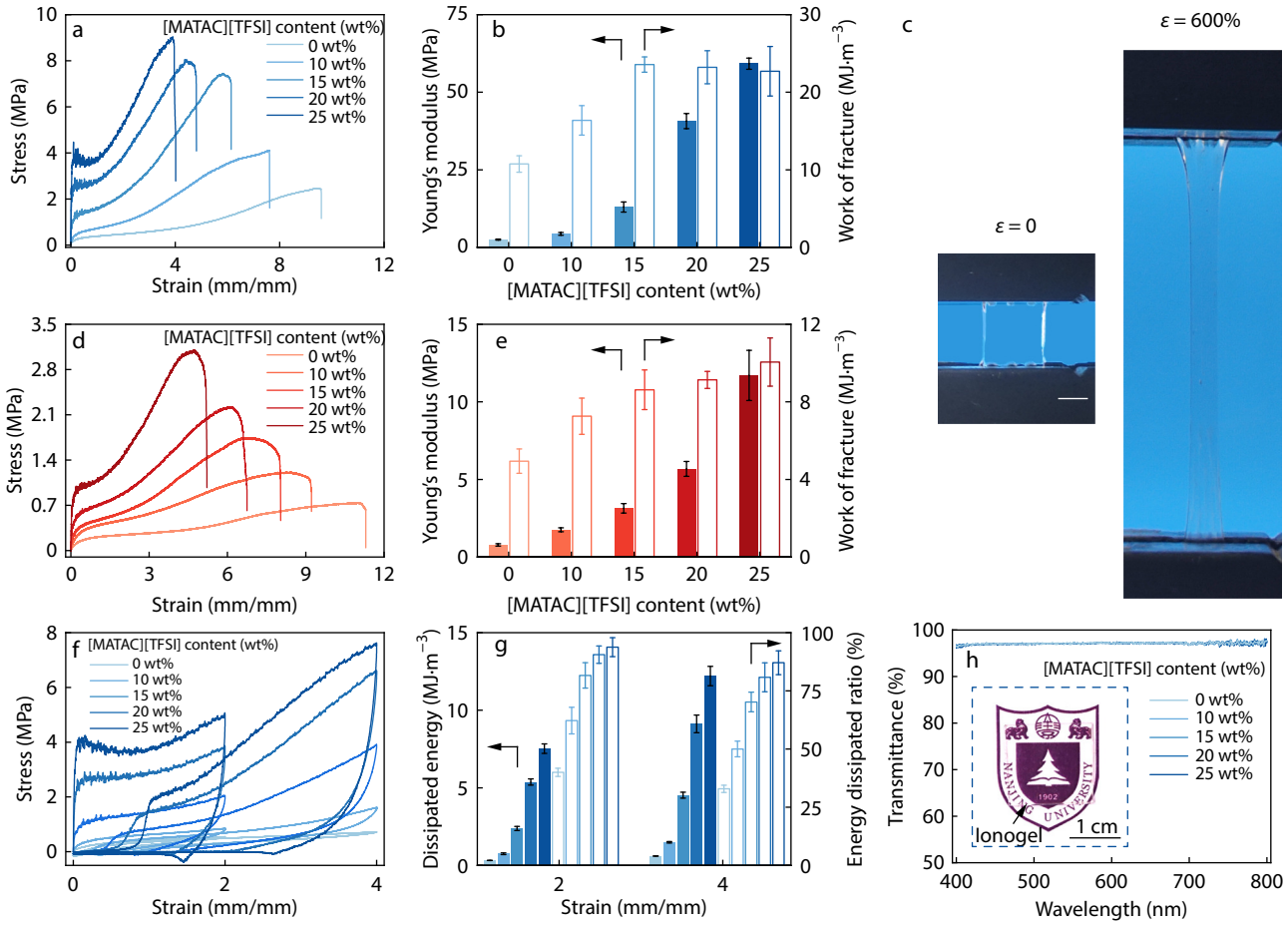

Fig. 3 Mechanical characterization of ionogels. (a) Stress-strain curves, (b) Young's modulus and fracture work of PEMAN ionogels; (c) Photos of the ionogel before and after stretching (Scale bar: 2 cm); (d) Stress-strain curves, (e) Young's modulus and fracture work of PEMMN ionogels; (f) Stress loading-unloading curves; (g) Dissipated energy and energy dissipated ratio of PEMAN ionogels; (h) Transmittance characterization and optical photos of PEMAN ionogels.

2.49 MPa (0 wt%) to 59.19 MPa (25 wt%). The work of fracture (area under the stress-strain curve) which reflecting energy absorption capacity reached a maximum of 23.57 MJ·m^{-3} at 15 wt% [MATAC][TFSI] (Fig. 3b). Fig. 3(c) displays photographs of the PEMAN ionogel with the highest work of fracture before and after stretching to 600% strain.

The PEMMN ionogels exhibited similar trends in mechanical properties to the PEMAN ionogels. However, because of the lower methacrylamide content, the density of hydrogen bonds in the PEMMN ionogels was significantly reduced, leading to lower strength and toughness compared to the PEMAN ionogels, albeit with slightly better extensibility. As shown in Fig. 3(d), the fracture stress of PEMMN ionogels increased from 0.73 MPa (0 wt%) to 3.09 MPa (25 wt%), while the maximum elongation decreased from 1130% to 520%. The reduced density of reversible energy-dissipating interactions in the PEMMN ionogels resulted in lower crosslinking strength and energy absorption than the PEMAN ionogels. For all tested compositions, Young's modulus and work of fracture increased monotonically with [MATAC][TFSI] content, ranging from 0.78 MPa to 11.70 MPa and reaching a maximum work of fracture of 10.05 MJ·m^{-3}, respectively (Fig. 3e). These results demonstrate that under the synergistic effect of abundant hydrogen bonds and ion-dipole interactions, the impact-resistant ionogels possess excellent and tunable mechanical properties, along with outstanding energy dissipation capabilities.

To further investigate the mechanical performance, we conducted notched sample tests to determine the critical strain for irreversible crack propagation, and measured the fracture toughness (energy dissipation per unit area during crack propagation). Figs. S3(a) and S3(b) (in ESI) present the typical toughness test data for the PEMAN and PEMMN ionogels, respectively. Noncovalent interactions in the ionogels act as sacrificial bonds to dissipate energy and inhibit crack propagation. Thus, under similar polymer network structures and crosslinking dynamics, a higher density of sacrificial bonds enhances crack resistance, leading to greater fracture toughness. As [MATAC][TFSI] content increased, the toughness of both PEMAN and PEMMN ionogels improved, reaching maximum values of 57.73 and 29.94 kJ·m^{-2}, respectively. The difference between the two likely stems from variations in the hydrogen bond density.

In addition, cyclic tensile tests were performed to evaluate the energy-dissipation performance. For PEMAN ionogels, a higher [MATAC][TFSI] content increased the ion-dipole inter-

https://doi.org/10.1007/s10118-025-3388-5

action density, leading to greater energy dissipation at the same strain (Fig. 3f). At 200% strain, dissipated energy increased from 0.32 MJ·m^{-3} to 7.52 MJ·m^{-3}, while at 400% strain, it rose from 0.61 MJ·m^{-3} to 12.21 MJ·m^{-3}. The energy dissipation ratio (ratio of dissipated energy to stored energy) peaked at 93.78% (200% strain) and 87.10% (400% strain) for 25 wt% [MATAC][TFSI] (Fig. 3g). In contrast, PEMMN ionogels, with lower hydrogen bond density, exhibited reduced energy dissipation but followed the same trend, with values ranging from 0.17–0.78 MJ·m^{-3} (200% strain, 44.41%–72.95% dissipation ratio) to 0.32–3.53 MJ·m^{-3} (400% strain, 42.81%–77.94% dissipation ratio) (Fig. S3c and Fig. S3d in ESI). These findings confirm that the PEMAN and PEMMN ionogels not only possess excellent mechanical strength and extensibility, ensuring structural stability under impact, but also exhibit superior energy dissipation capacity, which is crucial for impact resistance and protective applications.

While [MATAC][TFSI] primarily influences the ion-dipole interaction density, hydrogen bond density also plays a significant role in the mechanical performance. Thus, we adjusted the content of hydrogen-bonded monomers to study their effects. Using $PEM_{15}A_yN$ as a reference, we performed tensile tests at a fixed [MATAC][TFSI] content, while varying the acrylamide content. As shown in Fig. S4 (in ESI), a higher acrylamide content increased tensile strength but reduced extensibility, as more hydrogen bond donors enhanced crosslinking density and improved stiffness and fracture energy while limiting stretchability.

Owing to the strong intermolecular interactions, all the components in the impact-resistant ionogels were uniformly distributed within the network. Atomic force microscopy (AFM) phase imaging confirmed a homogeneous single-phase structure with ionic liquid solvents evenly dispersed throughout the polymer network without localized aggregation (Fig. S5 in ESI). Consequently, our ionogels exhibited high optical transparency, with an average visible light transmittance exceeding 94% at a thickness of 1 mm (Fig. 3h), demonstrating great potential for applications such as display protection and wearable visual devices where optical clarity is essential.

Dynamic Characteristics of Ionogels

The dynamic characteristics of materials are governed by their viscoelastic behavior, which can be quantitatively characterized through oscillatory rheological tests. Previous analyses have demonstrated that PEMAN and PEMMN ionogels share no fundamental differences in their network structures or interaction mechanisms. Therefore, in this and subsequent sections, we primarily used PEMAN ionogels (specifically, $PEM_{15}A_{10}N$ composition, unless otherwise stated) to investigate their physical properties.

First, we performed frequency-sweep oscillatory rheology tests on PEMAN ionogels at a constant strain (γ = 0.1%) and room temperature (25 °C), covering a frequency range of 0.1–100 Hz to examine their dynamic response from low to high frequencies. The rheological data for the PEMAN ionogels with varying [MATAC][TFSI] contents are shown in Fig. S6(a) (in ESI). We observed that both the storage modulus (G') and loss modulus (G'') increased with increasing [MATAC][TFSI] content, indicating stronger crosslinking networks and denser noncovalent interactions. Notably, across the tested frequency range, G' consistently exceeded G'', and both moduli increased with the frequency. The loss factor ($\tan\delta = G''/G'$) exhibited an initial decrease followed by an upward trend (Fig. S6b in ESI), confirming that, despite the absence of chemical crosslinkers, the ionogels remained in a rubbery state with a stable physical network. The loss factor reflects the damping performance of a material. In the 0.1–100 Hz range, $\tan\delta$ remained above 0.3, demonstrating the good damping properties of the ionogel.

Next, we characterized the temperature-dependent viscoelastic behavior of the PEMAN ionogels at 1 Hz. Both G' and G'' decreased with increasing temperature, indicating a loose network structure at elevated temperatures (Fig. S7 in ESI). The loss factor versus temperature plot clearly reveals the glass transition process and the corresponding glass transition temperatures T_g (Fig. 4a). As [MATAC][TFSI] content increased, T_g rose progressively from 39.7 °C to 49.6 °C, corroborated by differential scanning calorimetry (DSC) endothermic peaks (Fig. 4b). This trend arises because a higher [MATAC][TFSI] content increases the density of ion-dipole interactions, enhances crosslinking, and restricts chain segment mobility, ultimately leading to an increase in the glass transition temperature. It should be noted that the glass transition temperature obtained from rheological measurements can be influenced by factors such as the applied stress, frequency, and heating rate, and therefore may differ from the values measured by DSC. However, the trend in the glass transition temperature across different sample compositions is consistent between the two methods, which does not affect our conclusions. Additionally, owing to the stability of the physical crosslinking network and low volatility of the ionic liquid, the ionogel exhibited excellent thermal stability. Thermogravimetric analysis (TGA) results of the PEMAN ionogel demonstrate that significant decomposition only occurs when the temperature increases to approximately 300 °C (Fig. 4c), highlighting the potential's material for high-temperature applications.

Our impact-resistant ionogels, which are entirely composed of reversible noncovalent interactions, exhibit exceptional recoverability and self-healing capabilities. Cyclic tensile tests confirmed the ionogel recovery performance (Fig. 4d). After stretching to 400% strain and unloading, the second loading-unloading cycle revealed a higher stress-strain curve than the first unloading curve, indicating dynamic dissociation and reformation of non-covalent interactions during deformation. However, the dissipated energy in the second cycle is significantly lower, suggesting incomplete bond reformation within a short recovery time. Remarkably, heating the ionogel at 60 °C for 5 min fully restored its mechanical properties, as evidenced by nearly identical stress-strain curves in subsequent cycles. Moreover, as shown in Figs. 4(e) and 4(f), the ionogels rapidly reverted to their original shape after twisting, bending, or large-strain stretching. Physical crosslinking between the polymer chains preserves the initial shape, preventing irreversible deformation.

To evaluate the self-healing performance of the ionogel, notch-rejoining experiments were performed. Two PEMAN ionogel samples dyed with Coomassie Blue and Congo Red

https://doi.org/10.1007/s10118-025-3388-5

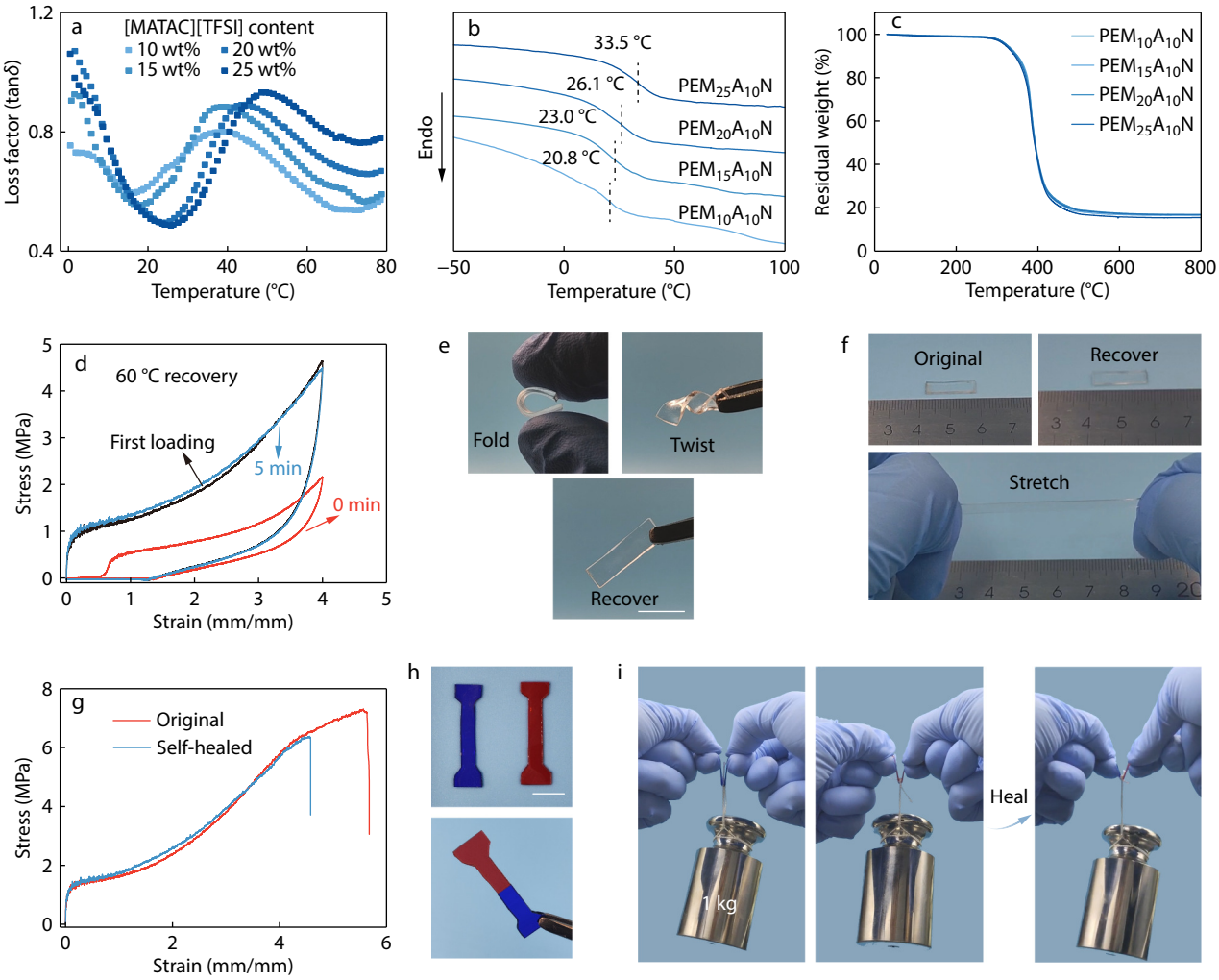

Fig. 4 The dynamic properties of ionogels. (a) Temperature dependence of the loss factor of the PEMAN ionogels; (b) Differential scanning calorimetry (DSC) and (c) thermogravimetric analysis (TGA) of the ionogels; (d) Recovery of ionogels in stress loading-unloading curves; Photos of the ionogel subjected to (e) folding, twisting, (f) stretching and recovery (Scale bar: 1 cm); (g) The stress-strain curves of the ionogel in original state and after self-healed; (h) Photos of the ionogels before notched and splice healing 30 s (Scale bar: 1 cm); (i) Photos of lifting the weight for the ionogels in original states and the rejoined ionogel after full splicing healing.

were cut and cross-joined. Hydrogen bonds and ion-dipole interactions reformed at the interface, enabling the two pieces to heal into a dual-colored sample (Fig. 4h). Heating at 60 °C accelerated molecular chain mobility, facilitating rapid healing. After heating at 60 °C for 2 h, tensile tests of healed samples showed stress-strain curves nearly overlapping with pristine samples, stretching up to about 450% strain before fracture (Fig. 4g). The recovery efficiency was calculated to be 80.4% based on the elongation at break. Minor premature failure was attributed to a slight misalignment at the interface owing to the high modulus of the material. Notably, the healed samples could lift weights 4000 times their own mass without breaking (Fig. 4i), demonstrating that the ionogel possessed excellent self-healing properties attributed to its supramolecular nature and highly dynamic chain associations.

Environment Tolerance and Recyclability of Ionogels

In humid environments, hydrophilic polymers absorb moisture from the surrounding environment owing to the concentration gradients.[55] The diffusion of polymer solvents and their exchange with external water molecules also contribute to the increased water content in the polymer. This significantly compromises the mechanical strength, stability, and electrical conductivity of polymers.

Our PEMAN ionogel employs polyacrylate as the primary polymer network, which resists swelling and deformation under humid conditions. Furthermore, fluorinated ionic incorporated into the system. Owing to the strong electronegativity, low polarizability, small van der Waals radius of fluorine atoms, and high bond strength of C—F bonds, fluorinated polymers exhibit low surface energy, minimal moisture absorption, high thermal stability, and chemical resistance.[56,57] Additionally, the C—F bond is a poor hydrogen bond acceptor and donor, meaning that water molecules have negligible interactions with fluorinated polymers. As a result, the PEMAN ionogel demonstrated exceptional resistance to aqueous environments.

First, we measured the water contact angles of the iono-

gels with varying [MATAC][TFSI] ionic liquid content. As shown in Fig. 5(a), despite the presence of positively charged and hydrophilic polar functional groups on the polymer chains, the PEMAN ionogel still exhibited hydrophobic properties with a water contact angle exceeding 90°. Increasing the [MATAC][TFSI] content increased the positive charge density on the polymer chains, leading to a slight reduction in the contact angle.

Using the $PEM_{15}A_{10}N$ ionogel as an example, we investigated its weight change in humid environments. Under 60% and 90% relative humidity, the weight of the PEMAN ionogel remained nearly unchanged, indicating no moisture absorption or solvent leakage/evaporation (Fig. 5b). The abundant ion-ion and ion-dipole interactions between the free ionic liquids and the polymer network effectively prevent ionic liquid leakage while maintaining the hydrophobic nature of the ionogel.

To further examine the ionogel's resistance and stability in solution environments, we immersed the PEMAN ionogels in pure water, NaCl solution, and HCl acidic solution and observed and weighed them at different intervals to assess the swelling behavior (Fig. 5c). As illustrated, the dense physical crosslinking within the hydrophobic polymer network and the presence of hydrophobic ionic liquids greatly suppressed water diffusion, resulting in no volume change even after seven days of swelling. With prolonged swelling, trace amounts of solution diffused into the ionogel. Hydrophobic interactions cause these solutions to aggregate, forming water-poor and water-rich phases within the ionogel, leading to reduced transparency and a transition from clear to gray-white.[58] Compared to the behavior in pure water, the swelling of the ionogel in an acidic solution exhibited some differences. In addition to the phase separation caused by the diffusion of water molecules, hydrolysis of ester groups under acidic conditions may also occur, which could further contribute to changes in the appearance of the sample. The photos show that the transparency of the ionogels swollen in water and acidic solutions reached its minimum by the third day, with

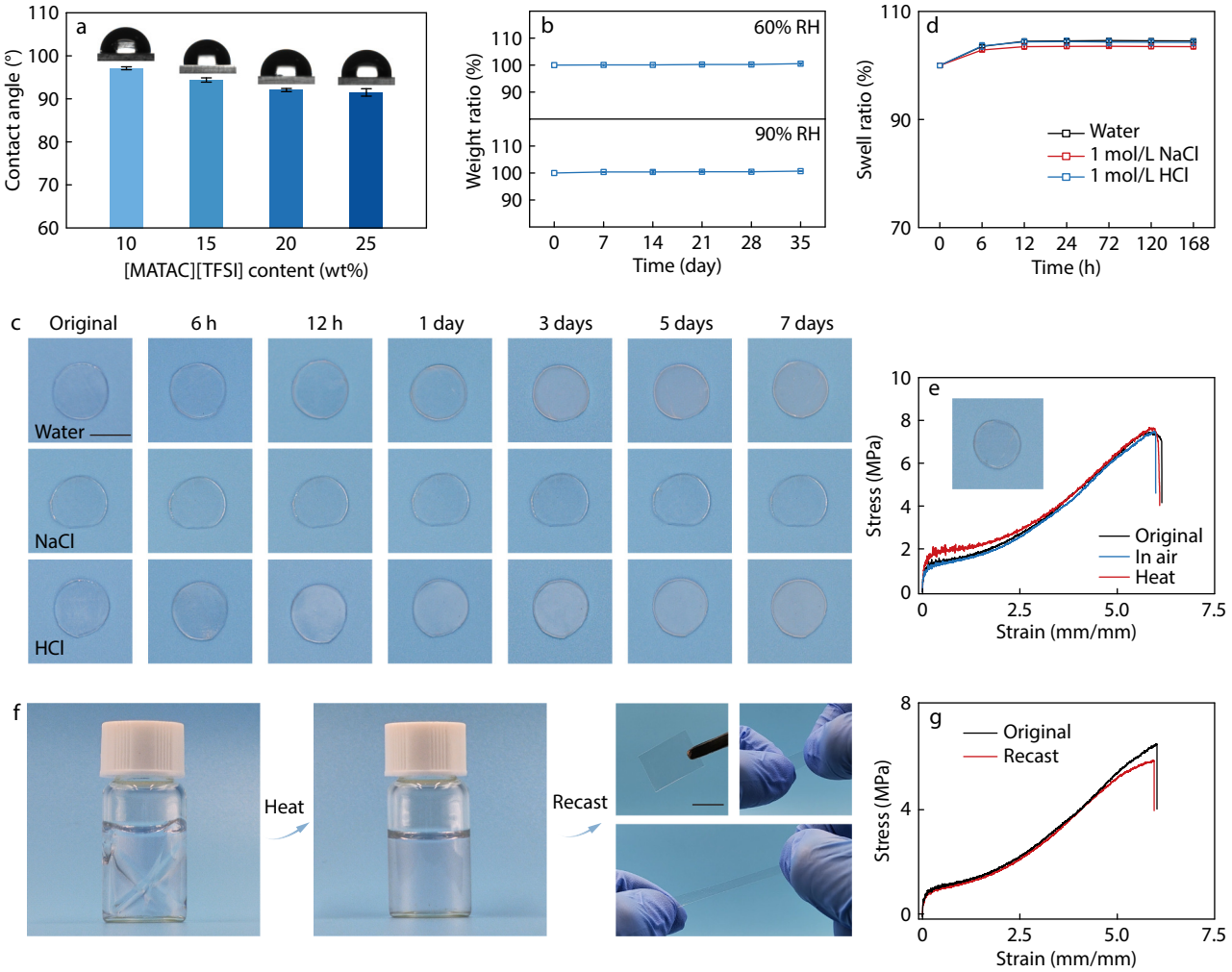

Fig. 5 Water tolerance and recyclability of ionogels. (a) The effect of [MATAC][TFSI] content on water contact angle; (b) The mass change of PEMAN ionogel in a humid environment; (c) Swelling photographs of PEMAN ionogels in different solvents (Scale bar: 1 cm) and (d) corresponding swelling ratio changes; (e) Comparison of mechanical properties among the initial state, humid environment storage, and heat-treated ionogel after water immersion (The picture inset is the heat-treated ionogel after water immersion for 7 days); (f) The recycling and reshaping process of ionogel (Scale bar: 1 cm) and (g) mechanical property comparison between reshaped samples and the initial state.

https://doi.org/10.1007/s10118-025-3388-5

little further change afterward. The mass ratio before and after swelling indicated that the swelling ratio peaked at this point, reaching equilibrium at 104.6% and 104.4%, respectively. Subsequent swelling led to a slight decrease in mass, likely due to minimal ionic liquid diffusion driven by the concentration gradients. Notably, the ionogel immersed in salt solution showed almost no change in transparency and exhibited a lower swelling ratio (103.6%) compared to the other groups, possibly due to the higher osmotic pressure of the salt solution, which reduced the water influx (Fig. 5d). Notably, in strongly alkaline solutions, irreversible hydrolysis of ester groups leads to significant swelling and eventual dissolution of the ionogel. Therefore, our ionogel was not suitable for use in alkaline environments.

These results confirm that the PEMAN ionogel maintains its structural and compositional stability in humid and aqueous environments. Subsequent mechanical testing confirmed that moisture exposure had a negligible impact on the performance, and any minor effects could be eliminated through simple treatment. Owing to the weak interactions between the ionogel and water molecules, the absorbed water can be removed *via* mild heat treatment. As shown in the Fig. 5(e), we compared the tensile mechanical properties of PEMAN ionogels in their initial state, after storage at 60% humidity at 25 °C, and after swelling in pure water followed by heat treatment. The gray-white ionogel regained transparency after heat treatment, with no significant degradation in the mechanical performance. This highlights the outstanding resistance of the ionogel to aqueous environments and its potential for humid-environment applications.

Because the PEMAN ionogel lacks chemical crosslinking between the polymer chains, it can be dissolved in a suitable solvent for recycling (Fig. 5f). As previously demonstrated, we selected low-boiling-point acetonitrile as the solvent. After heating, the PEMAN ionogel was completely dissolved in acetonitrile. The solution was then poured into a custom silicone mold, and after allowing acetonitrile to evaporate at room temperature, the PEMAN ionogel was recovered. The recycled ionogel exhibited mechanical properties nearly identical to those of the original ionogel (Fig. 5g), confirming a damage-free recycling method with significant cost savings and environmental benefits.

Impact Resistance Characteristic of Ionogels

The exceptional mechanical properties and energy dissipation capacity of the PEMAN ionogel endowed it with remarkable impact resistance. To characterize its impact performance, we conducted a series of impact-related experiments. A split Hopkinson pressure bar (SHPB) system was constructed to simulate high-speed impact conditions, and quasi-static compression tests were performed using a universal testing machine.

As shown in Fig. 6(a), the SHPB setup consists of a striker bar, incident bar, transmission bar, and damping components. The test specimen was sandwiched between incident and transmission bars. Upon pneumatic launch, the striker bar impacts the incident bar and transmits a force through the specimen to the transmission bar. During this process, the energy dissipated by the PEMAN ionogel was calculated using strain gauges on the incident and transmission bars, with the impact velocity controlled by air pressure.

High-speed compression tests were conducted at various strain rates (Fig. 6b). The results demonstrated that both the impact stress and strain of the PEMAN ionogel increased progressively with higher striker velocities. The ionogel exhibited high toughness and compressibility and effectively resisted external impacts through deformation-mediated energy dissipation. Under greater impact forces, the ionogel develops larger compressive strains to dissipate energy, resulting in enhanced impact toughness (defined as the area enclosed by the stress-strain curve under high-speed impact). At a strain rate of 9000 s^{-1}, the PEMAN ionogel reaches maximum stress and strain values, enduring 161.6 MPa stress at 73.7% compression while achieving 80.3 $MJ{\cdot}m^{-3}$ impact toughness (Figs. S8a and S8b in ESI).

For comparison, PEAN ionogels (lacking ion-dipole interactions) and PEMN ionogels (lacking hydrogen bonds) were tested under identical conditions. The PEMAN ionogel significantly outperformed the modulus, load-bearing capacity, and impact toughness at similar strain rates (Fig. S9 in ESI). This confirms that the synergistic combination of hydrogen bonding and ion-dipole interactions in the PEMAN ionogels enables superior energy dissipation under high-speed impacts, allowing greater stress resistance and load tolerance. Quasi-static compression tests yielded analogous results in that PEMAN ionogels demonstrated superior energy dissipation performance, further validating the energy dissipation advantages of this cooperative interaction mechanism (Figs. 6c, S10, and S11 in ESI).

Additional experiments were designed to visually demonstrate impact resistance. Highly elastic polymers, such as PDMS, store and release impact energy through rebound, potentially causing vibrational damage. In contrast, the non-covalent interactions of the PEMAN ionogel dissociated during deformation, dissipating most of the impact energy with minimal rebound. As shown in Fig. 6(d), we defined the rebound ratio as the height ratio between a dropped ball and its rebound, with the height difference representing the absorbed energy. While PDMS exhibits substantial rebound due to its elasticity, the PEMAN ionogel absorbs most of the kinetic energy (Fig. 6e), limiting the ball rebound to about 10% across different drop heights, significantly outperforming PDMS in damping efficiency (Fig. 6f).

Practical applications were evaluated using the PEMAN ionogels as protective layers. When a fragile beaker was dropped from 0.8 m onto a 1 mm thick PEMAN film, it rebounded slightly without damage (Fig. 6g). The ionogel also mitigated energy penetration. The 1 mm thickness PEMAN layer on quartz glass prevented breakage from a 0.3 m ball drop, whereas the unprotected glass shattered (Fig. 6h). These tests visually confirmed the exceptional protective performance of the ionogels. Finally, steel ball impact tests quantified the protection effectiveness *via* G-force reduction. The 0.2 mm PEMAN layer reduced peak impact force by about 40% for drops from 0.2 m (Fig. 6i). In addition, we conducted drop-weight impact tests with an initial impact energy of 20 J (Fig. S12 in ESI). Under this much higher impact energy, which significantly exceeded that of the ball drop test, our ionogel still exhibited excellent damping performance, underscoring the outstanding damping capability of our ionogel.

https://doi.org/10.1007/s10118-025-3388-5

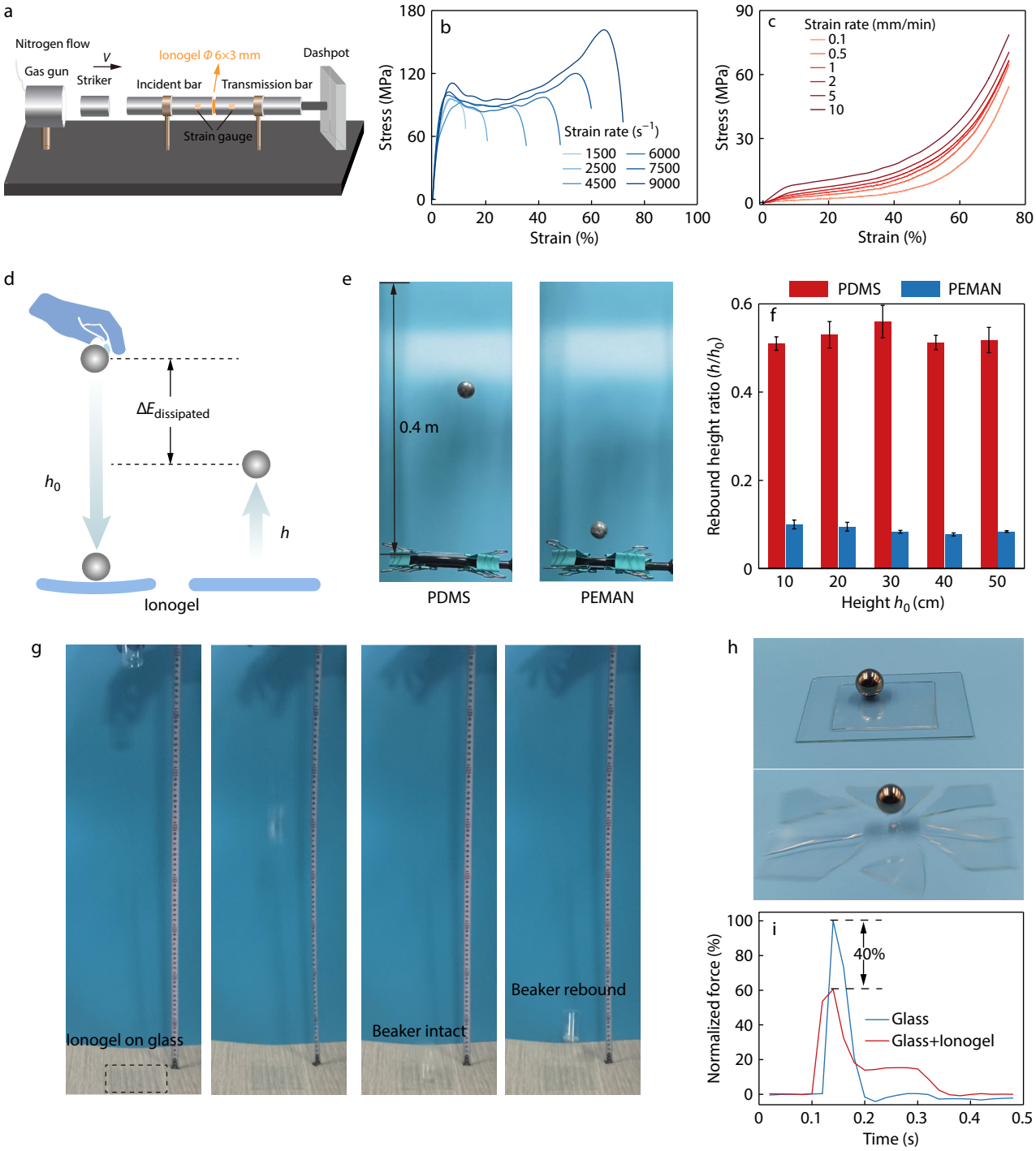

Fig. 6 Impact resistance characterization of ionogels. (a) Schematic illustration of the SPHB testing system; (b) Compression stress-strain curves of PEMAN ionogels at different strain rates; (c) Quasi-static compression tests of PEMAN ionogels at different strain rates; (d) Schematic illustration of the (e) comparison of steel ball rebound height when PDMS elastomer and PEMAN ionogels are used as buffer layer; (f) The rebound of the ball at different falling heights; (g) Snapshots of beaker impacting the PEMAN ionogel that dropped from 0.8 m height (Ionogel thickness: 1 mm); (h) Comparison of glass impact resistance with/without the PEMAN ionogel protection under ball impact testing; (i) Peak G-force measurement comparison in free-fall ball impact experiments with/without the PEMAN ionogel shock-absorbing layer.

CONCLUSIONS

In this study, we developed a tough, transparent, and self-healing ionogel that combines mechanical robustness, environmental resilience, and exceptional impact resistance within a single-material system. Through the rational integration of dynamic hydrogen bonding and ion-dipole interactions, the material overcomes longstanding trade-offs in soft material design,

https://doi.org/10.1007/s10118-025-3388-5

achieving both high fracture toughness and rapid self-recovery under mild conditions.

Computational analysis and experiments confirmed the molecular basis of these properties; hydrogen bonds contribute to energy dissipation and reformation as strong, thermally stable physical crosslinks. The ion-dipole interactions not only further enhance the mechanical properties, but also preserve the dynamic and self-healing characteristics of the material. Together, these reversible interactions form a supramolecular network capable of withstanding large deformations and severe mechanical impacts while remaining processable, recyclable, and stable in humid, saline, and acidic environments.

Beyond providing fundamental insights into supramolecular design, this ionogel offers practical advantages for emerging applications. Its excellent impact-damping properties, combined with its high optical transparency and environmental stability, make it a promising candidate for flexible protective coatings, wearable electronics, soft robotics, and transparent structural materials. This straightforward one-step synthesis route also facilitates large-scale fabrication and integration with diverse substrates. Moreover, the molecular design principles demonstrated here can be expanded further. By introducing stimuli-responsive components (*e.g.*, thermochromic or conductive fillers), ionogels can be adapted for multifunctional devices such as sensors, actuators, or adaptive interfaces. In addition, tailoring ionic liquid chemistry may enable tunable adhesion, electrical conductivity, or underwater operability, broadening its impact across materials science and engineering.

Altogether, this work provides not only a high-performance material but also a generalizable strategy for designing next-generation soft materials that combine strength, resilience, and adaptability through cooperative supramolecular interactions.

Conflict of Interests

The authors declare no interest conflict.

Electronic Supplementary Information

Electronic supplementary information (ESI) is available free of charge in the online version of this article at http://doi.org/10.1007/s10118-025-3388-5.

Data Availability Statement

Data supporting the findings of this study are available from the corresponding author upon reasonable request. Author's contact information: leihai@zju.edu.cn; caoyi@nju.edu.cn.

ACKNOWLEDGMENTS

This work was financially supported by the National Natural Science Foundation of China (Nos. T2222019 and T2225016), the National Key R&D Program of China (No.2024YFA0919300) and the Fundamental Research Funds for the Central Universities (Nos. 020414380232 and 021414380534).

REFERENCES

1 Qiao, H.; Wu, B.; Sun, S.; Wu, P. Entropy-driven design of highly impact-stiffening supramolecular polymer networks with salt-bridge hydrogen bonds. *J. Am. Chem. Soc.* **2024**, *146*, 7533–7542.
2 Wang, W.; Wang, S.; Zhou, J.; Deng, H.; Sun, S.; Xue, T.; Ma, Y.; Gong, X. Bio-inspired semi-active safeguarding design with enhanced impact resistance *via* shape memory effect. *Adv. Funct. Mater.* **2023**, *33*, 2212093.
3 Cheng, Y.; Zhang, X.; Qin, Y.; Dong, P.; Yao, W.; Matz, J.; Ajayan, P. M.; Shen, J.; Ye, M. Super-elasticity at 4 K of covalently crosslinked polyimide aerogels with negative Poisson's ratio. *Nat. Commun.* **2021**, *12*, 4092.
4 Khaheshi, A.; Gorb, S.; Rajabi, H. Triple stiffness: a bioinspired strategy to combine load-bearing, durability, and impact-resistance. *Adv. Sci.* **2021**, *8*, 2004338.
5 Wu, W.; Cao, X.; Zou, J.; Ma, Y.; Wu, X.; Sun, C.; Li, M.; Wang, N.; Wang, Z.; Zhang, L. Triboelectric nanogenerator boosts smart green tires. *Adv. Funct. Mater.* **2019**, *29*, 1806331.
6 Tang, F.; Dong, C.; Yang, Z.; Kang, Y.; Huang, X.; Li, M.; Chen, Y.; Cao, W.; Huang, C.; Guo, Y.; Wei, Y. Protective performance and dynamic behavior of composite body armor with shear stiffening gel as buffer material under ballistic impact. *Compos. Sci. Technol.* **2022**, *218*, 109190.
7 Portela, C. M.; Edwards, B. W.; Veysset, D.; Sun, Y.; Nelson, K. A.; Kochmann, D. M.; Greer, J. R. Supersonic impact resilience of nanoarchitected carbon. *Nat. Mater.* **2021**, *20*, 1491–1497.
8 Selim, M. S.; El-Safty, S. A.; Shenashen, M. A.; Elmarakbi, A. Advances in polymer/inorganic nanocomposite fabrics for lightweight and high-strength armor and ballistic-proof materials. *Chem. Eng. J.* **2024**, *493*, 152422.
9 Cheng, J.; Yao, X.; Zhang, Z.; Tan, Y.; Hu, N.; Ma, C.; Zhang, G. Intelligent anti-impact elastomers by precisely tailoring the topology of modular polymer networks. *Mater. Horiz.* **2024**, *11*, 3143–3156.
10 Wang, Z.; Wang, Z.; Li, D.; Yang, C.; Zhang, Q.; Chen, M.; Gao, H.; Wei, L. High-quality semiconductor fibres *via* mechanical design. *Nature* **2024**, *626*, 72–78.
11 Xiang, H.; Li, X.; Wu, B.; Sun, S.; Wu, P. Highly damping and self-healable ionic elastomer from dynamic phase separation of sticky fluorinated polymers. *Adv. Mater.* **2023**, *35*, 2209581.
12 Zhou, S.; Zhao, Y.; Zhang, K.; Xun, Y.; Tao, X.; Yan, W.; Zhai, W.; Ding, J. Impact-resistant supercapacitor by hydrogel-infused lattice. *Nat. Commun.* **2024**, *15*, 6481.
13 Ma, K.; Yi, H.; Gao, Y.; Cao, Y.; Ge, K.; Kuang, T.; Ji, H.; Li, M.; Feng, H. High-sensitivity and damage redundant detection capable gel-state [BMIM][BF_4] electronic skin for aerospace applications. *Supramol. Mater.* **2024**, *3*, 100077.
14 Liao, S.; Lian, X.; Wang, Y. Self-healing ionic liquid-based electronics and beyond. *Chinese J. Polym. Sci.* **2021**, *39*, 1235–1245.
15 Zhu, Q.; Liao, W.; Sun, C.; Qin, X.; Zhang, F.; Ji, H.; Li, Y.; Wen, Z.; Sun, X. Highly stretchable, conductive, and wide-operating temperature ionogel based wearable triboelectric nanogenerator. *Nano Res.* **2023**, *16*, 11638–11645.
16 Lei, B.; Cao, L.; Qu, X.; Liu, Y.; Shao, J.; Wang, Q.; Li, S.; Wang, W.; Dong, X. Thermal-sensitive ionogel with NIR-light controlled adhesion for ultrasoft strain sensor. *Nano Res.* **2023**, *16*, 5464–5472.
17 Li, Q.; Li, W.; Liu, Z.; Zheng, S.; Wang, X.; Xiong, J.; Yan, F. Poly(ionic liquid) double-network elastomers with high-impact resistance enhanced by cation-π interactions. *Adv. Mater.* **2024**, *36*, 2311214.
18 Fang, Y. H.; Liang, C.; Liljeström, V.; Lv, Z. P.; Ikkala, O.; Zhang, H. Toughening hydrogels with fibrillar connected double networks.

Adv. Mater. **2024**, *36*, 2402282.
19 Zhao, L. J.; Tang, N.; Wang, X. T.; Li, M. H.; Hu, J. Conductive polyaniline hydrogel featuring high toughness and low hysteresis. *Chinese J. Polym. Sci.* **2025**, *43*, 581–587.
20 Li, L.; Lei, H.; Cao, Y. Fatigue-resistant hydrogels. *Chem. Res. Chin. Univ.* **2024**, *40*, 64–77.
21 Yang, K.; Guan, J.; Numata, K.; Wu, C.; Wu, S.; Shao, Z.; Ritchie, R. O. Integrating tough Antheraea pernyi silk and strong carbon fibres for impact-critical structural composites. *Nat. Commun.* **2019**, *10*, 3786.
22 Yan, D.; Luo, J.; Wang, S.; Han, X.; Lei, X.; Jiao, K.; Wu, X.; Qian, L.; Zhang, X.; Zhao, X.; Di, J.; Zhang, Z.; Gao, Z.; Zhang, J. Carbon nanotube-directed 7 GPa heterocyclic aramid fiber and its application in artificial muscles. *Adv. Mater.* **2024**, *36*, 2306129.
23 Yin, J. F.; Xiao, H.; Xu, P.; Yang, J.; Fan, Z.; Ke, Y.; Ouyang, X.; Liu, G. X.; Sun, T. L.; Tang, L.; Cheng, S. Z. D.; Yin, P. Polymer topology reinforced synergistic interactions among nanoscale molecular clusters for impact resistance with facile processability and recoverability. *Angew. Chem. Int. Ed.* **2021**, *60*, 22212–22218.
24 Zhou, X.; Yin, J. F.; Chen, C.; Chi, Y.; Chen, J.; Liu-Fu. W.; Yang, J.; Long, S.; Tang, L.; Yao, X.; Yin, P. Hierarchical supramolecular aggregation of molecular nanoparticles for granular materials with ultra high-speed impact-resistance. *Adv. Sci.* **2024**, *11*, 2405285.
25 Wu, J.; Wu, B.; Xiong, J.; Sun, S.; Wu, P. Entropy-mediated polymer–cluster interactions enable dramatic thermal stiffening hydrogels for mechanoadaptive smart fabrics. *Angew. Chem. Int. Ed.* **2022**, *61*, e202204960.
26 Huang, W.; Shishehbor, M.; Guarín-Zapata, N.; Kirchhofer, N. D.; Li, J.; Cruz, L.; Wang, T.; Bhowmick, S.; Stauffer, D.; Manimunda, P.; Bozhilov, K. N.; Caldwell, R.; Zavattieri, P.; Kisailus, D. A natural impact-resistant bicontinuous composite nanoparticle coating. *Nat. Mater.* **2020**, *19*, 1236–1243.
27 Liu, M.; Wan, X.; Yang, M.; Wang, Z.; Bao, H.; Dai, B.; Liu, H.; Wang, S. Thermo-responsive jamming of nanoparticle dense suspensions towards macroscopic liquid–solid switchable materials. *Angew. Chem. Int. Ed.* **2022**, *61*, e202114602.
28 Wang, H.; Cheng, L.; Yu, J.; Si, Y.; Ding, B. Biomimetic Bouligand chiral fibers array enables strong and superelastic ceramic aerogels. *Nat. Commun.* **2024**, *15*, 336.
29 Wen, S. M.; Chen, S. M.; Gao, W.; Zheng, Z.; Bao, J. Z.; Cui, C.; Liu, S.; Gao, H. L.; Yu, S. H. Biomimetic gradient Bouligand structure enhances impact resistance of ceramic-polymer composites. *Adv. Mater.* **2023**, *35*, 2211175.
30 Liang, X.; Chen, G.; Lei, I. M.; Zhang, P.; Wang, Z.; Chen, X.; Lu, M.; Zhang, J.; Wang, Z.; Sun, T.; Lan, Y.; Liu, J. Impact-resistant hydrogels by harnessing 2D hierarchical structures. *Adv. Mater.* **2023**, *35*, 2207587.
31 Yuan, F.; Zhang, X.-X.; Wu, K.; Li, Z.; Lin, Y.; Liang, X.; Yang, Q.; Liu, T. Damping chitin hydrogels by harnessing insect-cuticle-inspired hierarchical structures. *Cell Rep. Phys. Sci.* **2023**, *4*, 101644.
32 Huang, J.; Zhou, H.; Zhang, L.; Zha, H.; Shi, W.; Zhao, T.; Liu, M. Bioinspired stiff-soft gradient network structure for high-performance impact-resistant elastomers. *Giant* **2024**, *19*, 100320.
33 Tang, Y.; Wu, B.; Li, J.; Lu, C.; Wu, J.; Xiong, R. Biomimetic structural hydrogels reinforced by gradient twisted plywood architectures. *Adv. Mater.* **2025**, *37*, 2411372.
34 Lin, H.; Chen, H.; Liu, J.; Li, H.; Mao, D. Towards sturdy and sensable pressure-sensitive adhesive through hierarchical supramolecular interaction. *Supramol. Mater.* **2023**, *2*, 100047.
35 Chouhdry, H. H.; Lee, D. H.; Bag, A.; Lee, N. E. A flexible artificial chemosensory neuronal synapse based on chemoreceptive ionogel-gated electrochemical transistor. *Nat. Commun.* **2023**, *14*, 821.
36 Huang, X.; Li, L.; Zhu, H.; Lv, T.; Tang, L.; Shentu, Z.; Li, H.; Gao, T.; Zhang, K.; Hu, J.; Wang, W.; Xue, B.; Lei, H.; Cao, Y. Designing high-damping, optically clear ionogels through competitive binding for flexible and impact-resistant applications. *ACS Appl. Mater. Interfaces* **2025**, *17*, 9830–9840.
37 Zhu, Y.; Guo, Y.; Cao, K.; Zeng, S.; Jiang, G.; Liu, Y.; Cheng, W.; Bai, W.; Weng, X.; Chen, W.; Zhao, D.; Yu, H.; Yu, G. A general strategy for synthesizing biomacromolecular ionogel membranes via solvent-induced self-assembly. *Nat. Synth.* **2023**, *2*, 864–872.
38 Luo, X.; Chen, C.; He, Z.; Wang, M.; Pan, K.; Dong, X.; Li, Z.; Liu, B.; Zhang, Z.; Wu, Y.; Ban, C.; Chen, R.; Zhang, D.; Wang, K.; Wang, Q.; Li, J.; Lu, G.; Liu, J.; Liu, Z.; Huang, W. A bionic self-driven retinomorphic eye with ionogel photosynaptic retina. *Nat. Commun.* **2024**, *15*, 3086.
39 Wang, M.; Zhang, P.; Shamsi, M.; Thelen, J. L.; Qian, W.; Truong, V. K.; Ma, J.; Hu, J.; Dickey, M. D. Tough and stretchable ionogels by in situ phase separation. *Nat. Mater.* **2022**, *21*, 359–365.
40 Wang, J.; Zhang, S.; Li, L.; Wang, X.; Xiong, J.; Li, Q.; Li, W.; Yan, F. Glassy ionogels with high compressibility and strength for impact protection. *Proc. Natl. Acad. Sci. U. S. A.* **2025**, *122*, e2417978122.
41 Yang, M.; Li, J.; Wang, C.; Yang, L.; Fan, Z.; Wang, W.; Liu, G.; Cheng, L.; Qu, S.; Zhang, Z.; Zou, J.; Yu, W.; Gu, G.; Yan, X. Robust mechanically interlocked network ionogels. *Angew. Chem. Int. Ed.* **2025**, *64*, e202423847.
42 Peng, L.; Hou, L.; Wu, P. Synergetic lithium and hydrogen bonds endow liquid-free photonic ionic elastomer with mechanical robustness and electrical/optical dual-output. *Adv. Mater.* **2023**, *35*, 2211342.
43 Sigwalt, D.; Šekutor, M.; Cao, L.; Zavalij, P. Y.; Hostaš, J.; Ajani, H.; Hobza, P.; Mlinarić-Majerski, K.; Glaser, R.; Isaacs, L. Unraveling the structure-affinity relationship between cucurbit[n]urils (n = 7, 8) and cationic diamondoids. *J. Am. Chem. Soc.* **2017**, *139*, 3249–3258.
44 Yu, Z.; Wu, P. Underwater communication and optical camouflage ionogels. *Adv. Mater.* **2021**, *33*, 2008479.
45 Chen, J.; Gao, Y.; Shi, L.; Yu, W.; Sun, Z.; Zhou, Y.; Liu, S.; Mao, H.; Zhang, D.; Lu, T.; Chen, Q.; Yu, D.; Ding, S. Phase-locked constructing dynamic supramolecular ionic conductive elastomers with superior toughness, autonomous self-healing and recyclability. *Nat. Commun.* **2022**, *13*, 4868.
46 Wang, X.; Zhan, S.; Lu, Z.; Li, J.; Yang, X.; Qiao, Y.; Men, Y.; Sun, J. Healable, recyclable, and mechanically tough polyurethane elastomers with exceptional damage tolerance. *Adv. Mater.* **2020**, *32*, 2005759.
47 Wu, Z.; Chu, C.; Jin, Y.; Yang, L.; Qian, B.; Wang, Y.; Wang, Y.; Wu, J.; Jia, Y.; Zhang, W.; You, Z. Dynamic cross-linked topological network reconciles the longstanding contradictory properties of polymers. *Sci. Adv.* **2025**, *11*, eadt0825.
48 Cao, Y.; Morrissey, T. G.; Acome, E.; Allec, S. I.; Wong, B. M.; Keplinger, C.; Wang, C. A transparent, self-healing, highly stretchable ionic conductor. *Adv. Mater.* **2017**, *29*, 1605099.
49 Lee, M. J.; Han, J.; Lee, K.; Lee, Y. J.; Kim, B. G.; Jung, K. N.; Kim, B. J.; Lee, S. W. Elastomeric electrolytes for high-energy solid-state lithium batteries. *Nature* **2022**, *601*, 217–222.
50 Wen, K.; Xin, C.; Guan, S.; Wu, X.; He, S.; Xue, C.; Liu, S.; Shen, Y.; Li, L.; Nan, C. W. Ion-dipole interaction regulation enables high-performance single-ion polymer conductors for solid-state batteries. *Adv. Mater.* **2022**, *34*, 2202143.
51 Gao, L.; Jiang, W.; Zhang, X.; Sun, Y.; Chen, K.; Li, W.; Xie, H.; Liu, J. A self-healing poly(ionic liquid) block copolymer electrolyte enabled by synergetic dual ion-dipole interactions. *Chem. Eng. J.* **2024**, *479*, 147822.
52 Jin, Z.; Chen, T.; Liu, Y.; Feng, W.; Chen, L.; Wang, C. Multivalent

design of low-entropy-penalty ion-dipole interactions for dynamic yet thermostable supramolecular networks. *J. Am. Chem. Soc.* **2023**, *145*, 3526–3534.
53 Contreras-García, A.; Emilio, B.; Gilles, B.; Tom, C.; Angel, C.; and Alvarez-Lorenzo, C. Biofilm inhibition and drug-eluting properties of novel DMAEMA-modified polyethylene and silicone rubber surfaces. *Biofouling* **2011**, *27*, 123–135.
54 Zhang, X. N.; Du, C.; Wang, Y. J.; Hou, L. X.; Du, M.; Zheng, Q.; Wu, Z. L. Influence of the *α*-methyl group on elastic-to-glassy transition of supramolecular hydrogels with hydrogen-bond associations. *Macromolecules* **2022**, *55*, 7512–7525.
55 Wei, J.; Zheng, Y.; Chen, T. A fully hydrophobic ionogel enables highly efficient wearable underwater sensors and communicators. *Mater. Horiz.* **2021**, *8*, 2761–2770.
56 Yu, Z.; Wu, P. A highly transparent ionogel with strength enhancement ability for robust bonding in an aquatic environment. *Mater. Horiz.* **2021**, *8*, 2057–2064.
57 Boschet, F.; Ameduri, B. (Co)polymers of chlorotrifluoroethylene: synthesis, properties, and applications. *Chem. Rev*. **2014**, *114*, 927–980.
58 Xu, J.; Wu, B.; Hou, L.; Wu, P. Hydrogen bonding competition mediated phase separation with abnormal moisture-induced stiffness boosting. *Small* **2024**, *20*, 2401164.

https://doi.org/10.1007/s10118-025-3388-5